Chapter 7

Kinetics and Mechanisms of Metal Sorption at the Mineral–Water Interface

Donald L. Sparks[1], André M. Scheidegger[2], Daniel G. Strawn[1], and Kirk G. Scheckel[1]

[1]Department of Plant and Soil Sciences, University of Delaware, Newark, DE 19717–1303
[2]Waste Management Laboratory, Paul Scherrer Institut, CH-5232 Villigen, Switzerland

The rates and mechanisms of sorption reactions at the mineral/water interface are critical in determining the mobility, speciation, and bioavailability of metals in aqueous and terrestrial environments. This chapter discusses nonequilibrium aspects of metal sorption at the mineral/water interface, with emphasis on confirmation of slow sorption mechanisms using molecular approaches. It is shown that there is often a continuum between sorption processes, viz, diffusion, sites of varying energy states, and nucleation of secondary phases. For example, recent molecular level in-situ studies have shown that metal adsorption and "surface" precipitation can occur simultaneously.

Contamination of aqueous and terrestrial environments with metals and semi-metals derived from industrial, municipal, and agricultural sources is a major concern worldwide. Industries and government are spending millions of dollars determining what pollutants are present in contaminated soils and ground water and implementing strategies to remediate subsurface environments. In many cases, however, speciation of the metals is inaccurate and difficult and the mechanisms by which metals are retained in soils and aquatic systems over long periods of time are not understood.

Dynamic reactions in the subsurface environment are critical in affecting the fate and transport of metals, as well as a number of other important processes (Figure 1). Soils and sediments have a remarkable ability to sorb metals. Sorption reactions at the mineral/water interface significantly affect the mobility, speciation, and bioavailability of trace metal ions in aquatic and soil environments. Therefore, one must precisely understand the kinetics and mechanisms of metal sorption on mineral surfaces to accurately predict the fate of such pollutants in subsurface environments and to facilitate effective environmental remediation procedures.

Adsorption can be defined as the accumulation of a substance or material at an interface between the solid surface and the bathing solution. It is strictly a two-dimensional process and does not include three-dimensional processes such as "surface" precipitation, and diffusion into the sorbent structure. Although in

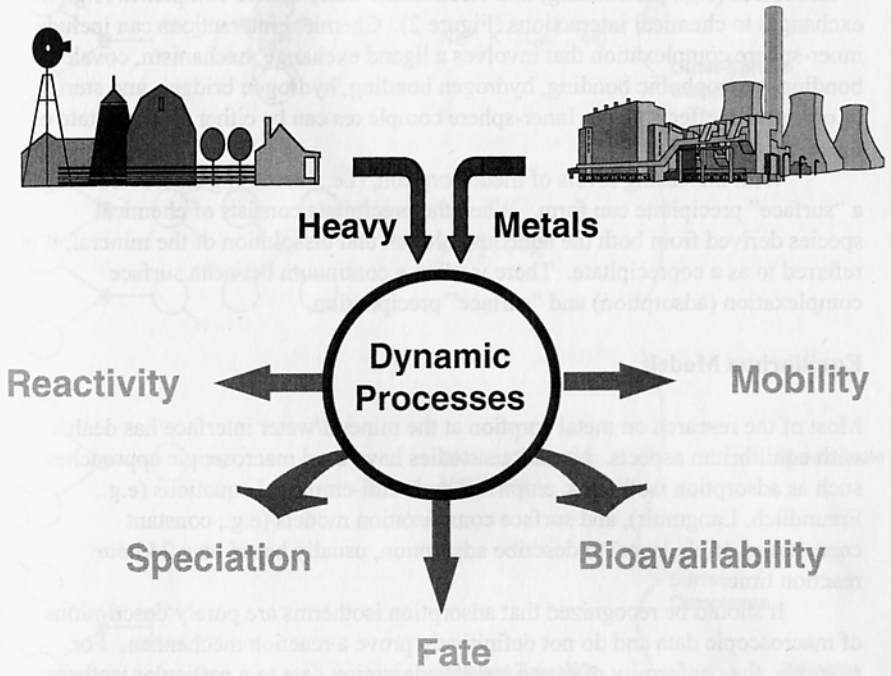

Figure 1. Metal reaction effects on processes in the subsurface environment.

many sorption studies spectroscopic techniques are used and reveal 3-dimensional products (as described later), it is often not clear whether a 3-dimensional process is actually occurring on a surface. To indicate this uncertainty, we will use the term "surface" precipitation. Adsorption, "surface" precipitation, and diffusion into the surface are collectively referred to as sorption, a general term that should be used when the retention mechanism at a surface is unknown. Although some scientists still use the term adsorption, sorption is a better term particularly when precipitation and absorption phenomena have not been eliminated as possible retention mechanisms.

The forces involved in adsorption can range from weak, physical, van der Waals forces (e.g., partitioning) and electrostatic outer-sphere complexes (e.g., ion exchange) to chemical interactions (Figure 2). Chemical interactions can include inner-sphere complexation that involves a ligand exchange mechanism, covalent bonding, hydrophobic bonding, hydrogen bonding, hydrogen bridges, and steric or orientation effects (*1,2*). Inner-sphere complexes can be either monodentate or bidentate (Figure 2).

With increasing levels of metal sorption, (i.e., increasing surface coverage) a "surface" precipitate can form. When the precipitate consists of chemical species derived from both the aqueous solution and dissolution of the mineral, it is referred to as a coprecipitate. There is often a continuum between surface complexation (adsorption) and "surface" precipitation.

Equilibrium Models

Most of the research on metal sorption at the mineral/water interface has dealt with equilibrium aspects. Numerous studies have used macroscopic approaches such as adsorption isotherms, empirical and semi-empirical equations (e.g., Freundlich, Langmuir), and surface complexation models (e.g., constant capacitance, triple layer) to describe adsorption, usually based on a 24 hour reaction time.

It should be recognized that adsorption isotherms are purely descriptions of macroscopic data and do not definitively prove a reaction mechanism. For example, the conformity of experimental adsorption data to a particular isotherm does not indicate that this is a unique description of the experimental data, and that only adsorption is operational. Thus, one cannot differentiate between adsorption and other sorption processes, such as "surface" precipitation, and diffusion using an adsorption isotherm, even though this has been done in the geochemistry literature.

Surface complexation models are chemical models that are based on molecular descriptions of the electric double layer using equilibrium derived adsorption data (*3*). Thus, no mechanistic information on sorption can be obtained. Surface complexation models often describe sorption data over a broad range of experimental conditions such as varying pH and ionic strength and have been used widely to describe metal cation and anion sorption reactions on metal (hydr)oxides, clays, and soils, and organic ligand and competitive sorption reactions on oxides. However, surface complexation models employ an array of

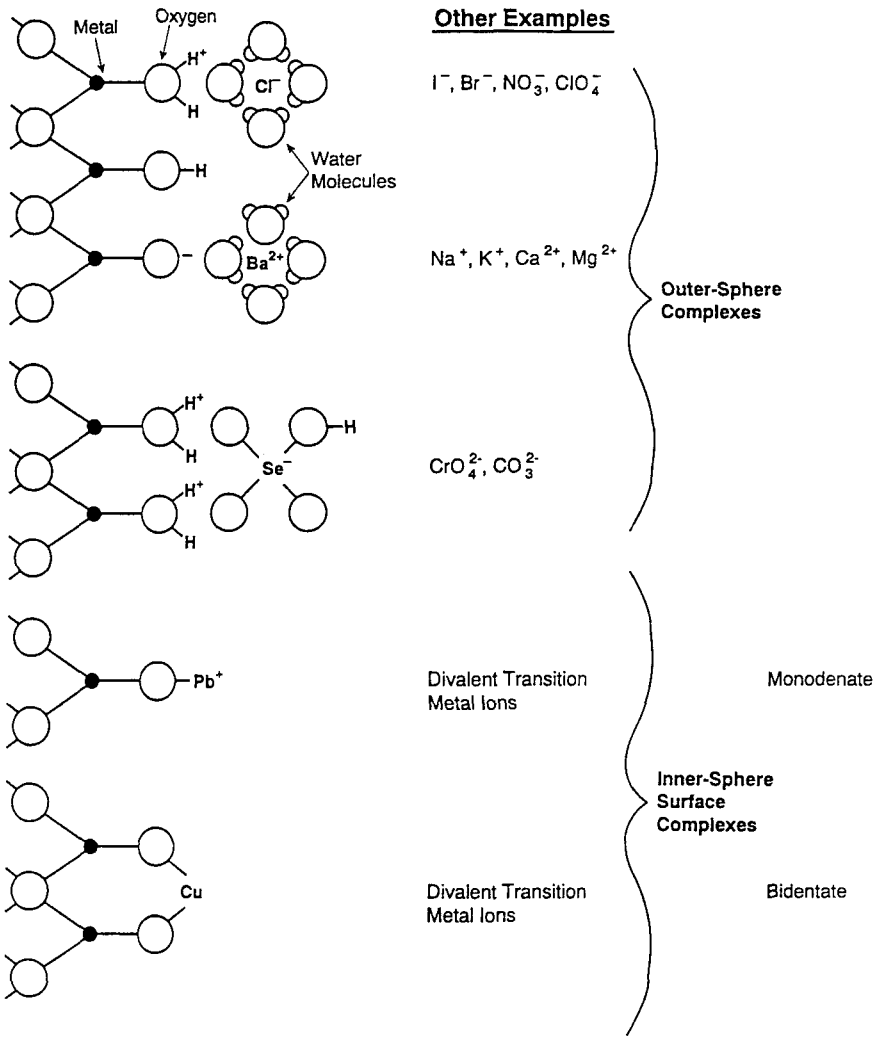

Figure 2. Schematic representation of surface complexes formed between inorganic ions and hydroxyl groups of an oxide surface. Modified from Hayes (*78*), with permission.

adjustable parameters to fit experimental data, and it has been shown that often several models may fit sorption data equally well (*4*).

Another major disadvantage of the commonly used surface complexation models, and of most equilibrium-based sorption models, is that three-dimensional surface products are not included as possible complexes. However, there are several exceptions. Farley et al. (*5*) and James and Healy (*6*) considered surface precipitation in successfully modeling sorption of hydrolyzable metal ions. Dzombak and Morel (*7*) modified the diffuse layer surface complexation model to include surface precipitation. However, these applications relied solely on macroscopic data without molecular-level identification of the sorption complex structure. Recently, Katz and Hayes (*8,9*) employed triple layer models, that included a surface solution model, a surface polymer model, and a surface continuum model to describe molecular level data for Co sorption on γ-Al_2O_3 over a wide range of surface coverages (0.1 to 100%).

Arguably, one of the major needs in modeling sorption on soils and natural materials is to include "surface" precipitation and other non-adsorption phenomena, based on molecular level data, as part of the model description and prediction. This is particularly important as recent research, based on in-situ spectroscopic analyses, indicates that metal-nucleation products form on an array of natural surfaces at low surface coverages and at relatively rapid time scales (*10-17*).

Kinetic and Molecular Approaches

In the past two decades, as concerns and interests about soil and water quality have increased, scientists and engineers have increasingly realized that reactions in subsurface environments are time-dependent. Kinetic studies can reveal something about reaction mechanisms at the mineral/water interface, particularly if energies of activation are calculated and stopped-flow or interruption techniques are employed. However, molecular and/or atomic resolution surface techniques should be employed to corroborate the proposed mechanisms hypothesized from equilibrium and kinetic studies. These techniques can be used either separately or, preferably, simultaneously with kinetic investigations (*2*).

There are two principal subdivisions in molecular spectroscopy: in-situ and non-in-situ methods (2,*18*). The principal invasive non-in-situ techniques used for soil and aquatic systems are x-ray photoelectron spectroscopy (XPS), auger electron spectroscopy (AES), and secondary mass spectroscopy (SIMS). Each of these techniques yields detailed information about the structure and bonding of minerals and the chemical species present on the mineral surfaces. XPS is one of the most widely used non-in-situ surface-sensitive techniques. It has been used to study sorption mechanisms of inorganic cations and anions such as Cu, Co, Ni, Cd, Cr, Fe, selenite, and uranyl in soil and aquatic systems (*19-28*). The disadvantage of invasive non-in-situ techniques is that they often must be performed under adverse experimental conditions, e.g., desiccation, high vacuum, heating, or particle bombardment. Such conditions may yield data that are misleading as a result of experimental artifacts (*2,29,30*). Review articles on XPS, AES, and SIMS are available (*29,31,32*).

In-situ methods require little or no alteration of the sample from its natural state (*2,18*). They can be applied to aqueous solutions or suspensions; most involve the input and detection of photons. Examples of in-situ techniques are electron paramagnetic resonance (EPR), Fourier-transform infrared (FTIR), nuclear magnetic resonance (NMR), x-ray absorption fine structure (XAFS), and Mössbauer spectroscopies. However, many other techniques are available (*2,33*).

XAFS has been heavily used to study the mechanisms of metal reactions at the mineral/water interface (*30, 33-37* and the chapter by Brown et al. in this volume for details on x-ray absorption spectroscopy and specific studies). While XAFS provides local chemical information, it provides no information on spatial resolution of surface species (*2*). Such information can only be obtained by microscopic methods. Scanning electron microscopy (SEM) and transmission electron microscopy (TEM or HRTEM - high resolution TEM) are well established methods for acquiring both chemical and micromorphological data on minerals and soils. TEM can provide information on spatial resolution of surface alterations and the amorphous nature or degree of crystallinity of sorbed species (ordering). It can also be combined with electron spectroscopies to determine elemental analysis (*2*). Scanning force microscopy (SFM) is also being increasingly used to study geochemical systems. SFM allows imaging of mineral surfaces in air or immersed in solution, and at subnanometer scale resolution (*40*). It has been applied to image mineral surfaces immersed in aqueous solutions, over the course of dissolution, precipitation, and nucleation reactions (*38-41* and the chapters by Hochella et al. and Maurice in this volume for detailed discussions).

Accordingly, to accurately predict the fate, mobility, speciation, and bioavailability of environmentally important metals and semi-metals in terrestrial and water environments, one must understand the kinetics and mechanisms of the reactions. This chapter focuses on nonequilibrium aspects of metal sorption/desorption and the confirmation of reaction mechanisms using in-situ atomic/molecular level spectroscopic and microscopic techniques.

Time Scales of Metal Sorption Reactions. Metal sorption reactions can occur over time scales ranging from milliseconds to several weeks depending on the sorbate/sorbent system. The type of sorbent can drastically affect the reaction rate. For example, sorption reactions are often more rapid on clay minerals such as kaolinite than on vermiculitic and micaceous minerals. This is in large part due to the availability of sites for sorption. Kaolinite has readily available planar external sites and sorption is often complete in minutes (*42*). Vermiculite and micas have multiple sites for retention of metals including planar, edge, and interlayer sites, with some of the latter sites being partially to totally collapsed. Consequently, sorption and desorption reactions on these sites can be slow. Often, an apparent equilibrium may not be reached even after several days or weeks. Thus, with vermiculite and mica, sorption can involve two to three different reaction rates - high rates on external sites, intermediate rates on edge sites, and low rates on interlayer sites (*43,44*).

The type of surface complex, i.e., outer-sphere versus inner-sphere (Figure

2), can also affect the rate and reversibility of metal sorption reactions. Outer-sphere complexation is usually rapid and reversible, whereas inner-sphere complexation is slower and may appear to be irreversible (*2*). Moreover, the rate of desorption from monodentate complexes may be higher than from bidentate complexes.

Metal sorption reactions on clay minerals, (hydr)oxides, humic substances and soils is usually characterized by a rapid, followed by a slow, reaction (Figure 3). The rapid reaction is ascribable to chemical reaction and film diffusion processes (*2,42*). For example, chemical reaction rates of metals on oxides occur on millisecond time scales (*45-47*). Half-times for divalent Cu, Pb, and Zn sorption on peat ranged from 5 to 15 seconds and were ascribed to film diffusion (*48*).

The slow metal sorption step on many minerals and soils occurs over time scales of days and longer. This slow sorption has been ascribed to several mechanisms including: interparticle or intraparticle diffusion in pores and solids, sites of low energy or reactivity, and "surface" precipitation/nucleation (*49-51*).

While it has been generally assumed that adsorption in comparison to "surface" precipitation is much more rapid, a recent study (*17*) has shown that "surface" precipitation processes can occur on time scales of minutes. The latter finding indicates that sorption and precipitation processes can occur simultaneously. However, in some cases, depending on reaction conditions and the metal involved, a particular sorption mechanism can dominate.

An important factor affecting the degree of slow sorption/desorption of metals is the time period the sorbate has been in contact with the sorbent (residence time). Ainsworth et al. (*52*) studied the sorption/desorption of Co, Cd, and Pb on hydrous ferric oxide (HFO) as a function of oxide aging and metal-oxide residence time. Oxide aging did not cause hysteresis of metal cation sorption-desorption. Increasing the residence time between the oxide and the metal cations resulted in hysteresis with Cd and Co but little hysteresis was observed with Pb. With Pb, between pH 3 and 5.5 there was slight hysteresis over a 21 week aging process (hysteresis varied from <2% difference between sorption and desorption to ≈ 10%). At pH 2.5 Pb desorption was complete within a 16 hour desorption period and was not affected by residence time (Figure 4). However, with Cd and Co (Figure 5), increasing hysteresis was observed as the metal/sorbent residence time increased from 2 to 16 weeks. After 16 weeks of aging 20% of the Cd and 53% of the Co was not desorbed, and even at pH 2.5, hysteresis was observed. The extent of reversibility with residence time for Co, Cd, and Pb was inversely proportional to the ionic radii of the ions, i.e., Co <Cd<Pb. Ainsworth et al. (*52*) attributed the hysteresis to Co and Cd incorporation into a recrystallizing solid (probably goethite) via isomorphic substitution and not to micropore diffusion.

Diffusion Mechanisms. Since minerals and soils are porous materials containing both macropores (>2nm) and micropores (<2nm) diffusion is a mechanism that can control the slow rate of metal sorption (Figure 6). These pores can be inter-particle (between aggregates) or intra-particle (within an individual particle).

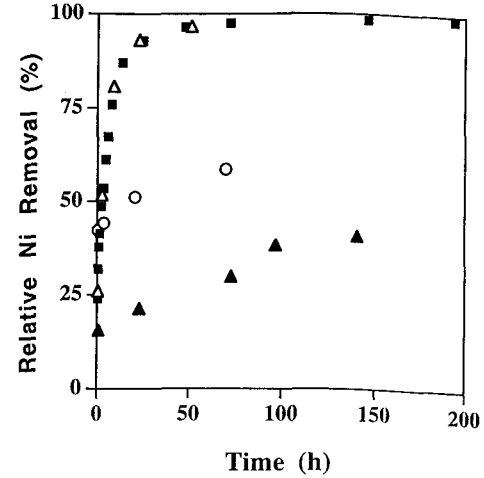

Figure 3. Kinetics of Ni sorption (%) on pyrophyllite (■), kaolinite (△), gibbsite (▲), and montmorillonite (o) from a 3 m*M* Ni solution at pH 7.5 and an ionic strength *I* = 0.1 *M*$NaNO_3$. The last sample of each experiment was collected and analyzed by XAFS. From Scheidegger et al. (*16*), with permission.

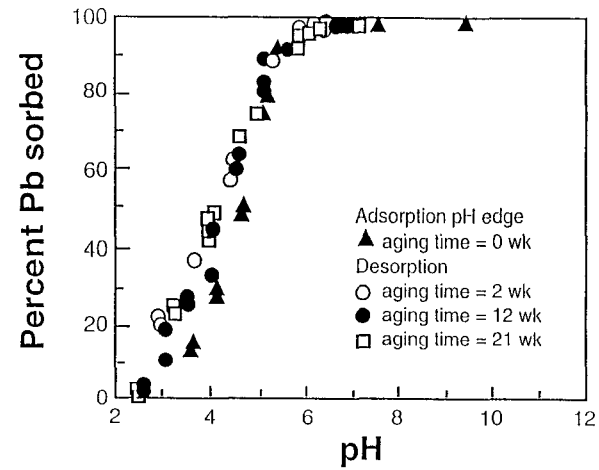

Figure 4. Fractional adsorption of Pb to hydrous Fe-oxide (HFO) as a function of pH and HFO-Pb aging time. From Ainsworth et al. (*52*), with permission.

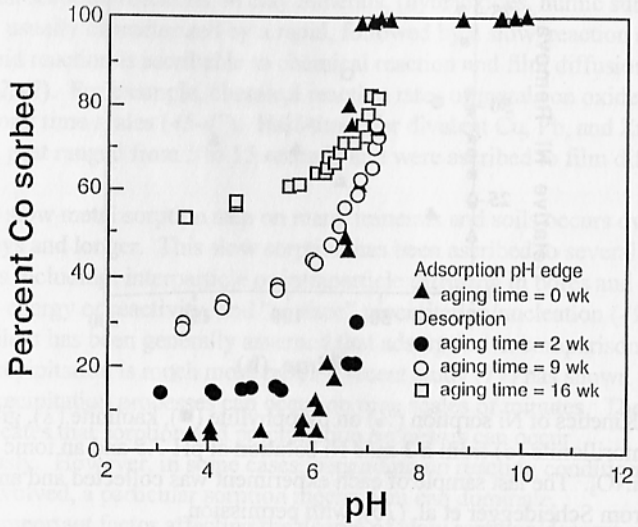

Figure 5. Fractional adsorption of Co to hydrous Fe-oxide (HFO) as a function of pH and HFO-Co aging time. From Ainsworth et al. (*52*), with permission.

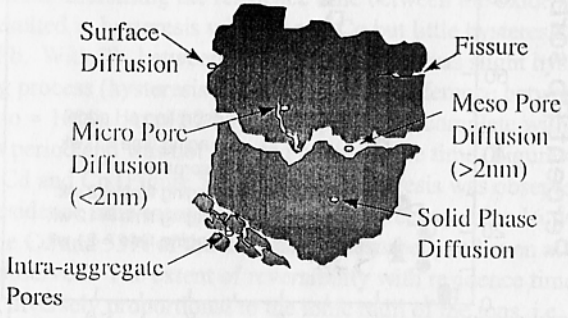

Figure 6. Diffusion processes in natural materials.

Intra-particle pores can form during weathering, upon solid formation, or may be partially collapsed interlayer space between mineral sheets, i.e., vermiculite and montmorillonite. The rate of diffusion through a pore is dependent on pore size, particle size, tortuosity, chemical interactions, chemical flux, and whether the pore is continuous or discontinuous. Besides pore diffusion, solid-phase diffusion is also a transport-limited process. Solid phase diffusion is dependent on the characteristics and interactions of the diffusant and the solid (*53*). Since there exists a range of diffusion rates in the soil, it follows that with increasing residence time the fraction of contaminants in the more remote areas of particles (accessible via slow diffusion) will increase. This slow sorption phenomenon is often the explanation researchers use to account for the slow continuous sorption and desorption observed between metals and natural materials (*42,50,54*).

Bruemmer et al. (*55*) studied Ni, Zn, and Cd sorption on goethite, a porous iron oxide known to have defects within the structure in which metals can be incorporated to satisfy charge imbalances. At pH 6, as reaction time increased from 2 hours to 42 days (at 293K), sorbed Ni increased from 12 to 70% of Ni removed from solution, and total increases in Zn and Cd sorption over this period increased 33 and 21%, respectively. The kinetics of Cd, Zn, and Ni were described well with a solution to Fick's second law (a linear relation with the square root of time). Bruemmer et al. (*55*) proposed that the uptake of the metal follows three-steps: (i) adsorption of metals on external surfaces; (ii) solid-state diffusion of metals from external to internal sites; and (iii) metal binding and fixation at positions inside the goethite particle. They suggest that the second step is the rate-limiting step. However, they did not conduct microscopic level experiments to confirm the proposed mechanism. In view of more recent studies, it is likely that the formation of metal-nucleation products could have caused the slow metal sorption reactions observed by Bruemmer et al. (*55*).

Similar observations on sorption of divalent metal ions were made by Coughlin and Stone (*56*). They hypothesized that the slow sorption and desorption on goethite was a result of slow pore diffusion. Axe and Anderson (*57*) also found that sorption of Cd and Sr could be characterized by a model which included two steps: a rapid reversible sorption step followed by a slow, rate-limiting process involving the diffusion of the cations through small pores existing along the surface.

While the above studies have suggested that diffusion is the rate-limiting step based on good model fits to data, macroscopic sorption experiments are not definitive proof of a mechanism (*50,58*). To give additional support to diffusion as a mechanism for sorption onto porous media, Papelis (*28*) measured surface coverages of Cd and selenite on porous aluminum oxides using XPS. He calculated the expected thickness of sorbed Cd and selenite from the total metal loss from solution using both external and internal surface areas. A good agreement was found between the calculated and the measured (using XPS) surface coverage thickness when the total surface area (i.e., internal and external surface area) was used. When the surface layer thickness was calculated without considering internal surface area, the calculated thickness exceeded the thickness observed using XPS. Therefore, the most likely sorption mechanisms were

sorption to external sites, diffusion of Cd into the internal structure, and subsequent sorption. While Papelis (*28*) did not measure the kinetics of the reaction, it seems probable that the sorption rate on the interior sites was lower than on the exterior sites, and thus a slow kinetic sorption step would exist.

Sites of Varying Energy States. Rates of metal sorption are also affected by sites of varying energy states (*50*). McBride (*59*) used EPR to study Cu sorption on noncrystalline aluminum oxide. He found that sorption involved sites of varying reactivity. The first reaction step involved the rapid sorption of a low quantity of Cu on high energy sites. A second reaction occurred over several weeks and resulted in the uptake of a greater amount of Cu and EPR spectra distinct from the first reaction step. Hayes and Leckie (*46*) and Grossl et al. (*47*) used pressure-jump relaxation to measure the kinetics of Pb sorption on aluminum oxide and Cu(II) sorption on goethite, respectively. They found that the best fit to the data was obtained by using a kinetic model that included a transformation from outer-sphere to inner-sphere complexation. Their data suggested that sorption behavior was biphasic, which they explained by suggesting that the slower reaction was a result of sites with lower affinities or energies. Lehmann and Harter (*60*) measured the kinetics of chelate promoted Cu^{2+} release from a soil to assess the strength of the bond formed. Sorption/desorption was biphasic, which was attributed to high and low energy bonding sites. With increased residence time from 30 minutes to 24 hours, Lehmann and Harter (*60*) speculated that there was a transition of Cu from low energy sites to higher energy sites (as evaluated by release kinetics). Incubations for up to four days showed a continued uptake of Cu and a decrease in the fraction released within the first three minutes, which was referred to as the low energy sorbed fraction.

"Surface" Precipitation and Polynuclear "Surface" Complex Formation. Recent studies using surface spectroscopic and microscopic techniques such as XAFS, EPR, XPS, AES, TEM, SEM and SFM have shown that the formation of "surface" precipitates and polynuclear "surface" complexes on natural materials are important sorption mechanisms (*10-12,14,16,17,26,27,35,61*).

Nucleation products of Co, Cr(III), Cu, Ni and Pb on oxides and aluminosilicates have been observed (*10-14,16,17,61-68*). Such products have been observed at metal surface loadings far below a theoretical monolayer coverage, and in a pH range below the pH where the formation of metal hydroxide precipitates would be expected according to the thermodynamic solubility product (*10-12,14,16,17*).

Three different types of nucleation products have been proposed: formation or sorption of polymers (dimers, trimers, etc.) on the surface (polynuclear surface complexes); a solid solution or coprecipitate that involves co-ions dissolved from the adsorbent; and a precipitate formed on the surface composed of ions from the bulk solution, or their hydrolysis products (*5,15,33,62,69*). The two latter products are examples of "surface" precipitates. In case the nucleation product is associated with the surface (polynuclear surface complexes), the process leads to the saturation of sites, whereas precipitation mechanisms create new reactive surface area.

The formation of metal nucleation products could be a significant cause of slow metal sorption on mineral surfaces. For example, XAFS results for Co sorption on rutile (TiO_2) showed an increase in the number of backscattering Co atoms for residence times of one day to 11 days, suggesting an increase in the size of nucleation products formed (*61*). However, similar results were not seen for Co aging on quartz (α-SiO_2). Data analysis of the Co/quartz system showed that the reaction time had no effect on the Co coordination environment and revealed the presence of a Co hydroxide-like "surface" precipitate even at a low surface loading.

The authors hypothesized that the reason for the observed slow change in the "surface" precipitate on rutile and not on quartz was a result of the similar radii between $^{VI}Co^{2+}$ (0.75Å) and $^{VI}Ti^{4+}$ (0.61Å); [Table I]. As a result, Co sorption on rutile was consistent with the formation of a precipitate that had similar lattice dimensions as the surface, effectively extending the lattice structure of the bulk solid, i.e., an epitaxial growth.

On quartz, however, the formation of a precipitate that has similar lattice dimensions as the surface is not favorable unless Co undergoes a coordination change from octahedral to tetrahedral. Such a coordination change is unlikely for Co in aqueous solution (*70*) and the XAFS spectra of the Co/quartz sorption system showed no evidence of a change. Thus, the Co hydroxide-like precipitate that formed on quartz was attached only to corners of selected Si tetrahedra on the surface.

Ni Sorption on Clay Minerals: A Case Study. Initial research with Co/clay mineral systems demonstrated the formation of nucleation products using XAFS spectroscopy, but the structure was not strictly identified and was referred to as a Co hydroxide-like structure (*11,12*). Thus, the exact mechanism for "surface" precipitate formation remained unknown. Recent research in our laboratory and elsewhere suggests that during sorption of Ni and Co metal ions, dissolution of the clay mineral or aluminum oxide surface can lead to precipitation of mixed Ni/Al and Co/Al hydroxide phases at the mineral/water interface (*14,16,17,67,71*). This process could act as a significant sink for metals in soils. The following discussion focuses on some of the recent research of our group on the formation kinetics of mixed cation hydroxide phases, using a combination of macroscopic and molecular approaches (*14-17*).

Figure 3 shows the kinetics of Ni sorption on pyrophyllite, kaolinite, gibbsite, and montmorillonite from a 3 m*M* Ni solution at pH = 7.5 (*16*). For kaolinite and pyrophyllite relative Ni removal from solution follows a similar sorption trend with ≈90% Ni sorbed within the first 24 hours. At the end of the experiments, relative Ni removal from solution was almost complete (Ni/kaolinite system, 97% sorbed after 70 hours; Ni/pyrophyllite system, 98% sorbed after 200 hours). Nickel sorption on gibbsite and montmorillonite exhibited a fast initial step. Thereafter, relative Ni removal from solution distinctively slowed down. Relative Ni sorption increased from 42-58% for the Ni/montmorillonite system (time range 0.5-70 hours) and from 15-41% for the Ni/gibbsite system (time range

1-140 hours). Although not shown, experiments with gibbsite and montmorillonite were carried out over longer times (up to 6 weeks).

Figure 7 illustrates the kinetics of Ni sorption on pyrophyllite, along with dissolved Si data from the Ni-treated pyrophyllite and from an untreated pyrophyllite (*16*). The release of Si into solution shows a similar kinetic behavior as Ni sorption on pyrophyllite. When one compares the Si release rate with the dissolution rate of the clay alone, the Si release rate in the Ni-treated system is strongly enhanced as long as Ni removal from solution is pronounced (Figure 7). Although not shown, a similar correlation between Ni sorption and Si release was observed for the Ni/kaolinite system but not for the Ni/montmorillonite system. The dissolution rate of the Ni/gibbsite system was not determined since the [Al] in solution was too low (<50 ppb) to produce reliable ICP measurements.

Figure 8 shows normalized, background-subtracted and k-weighted XAFS spectra of Ni sorbed on pyrophyllite, kaolinite, gibbsite, and montmorillonite (*16*). The XAFS samples were collected at the end of each experiment shown in Figure 3. The corresponding surface sorption densities, Γ's, were 3.1 μmol m^{-2} for pyrophyllite, 19.9 μmol m^{-2} for kaolinite, 5.0 μmol m^{-2} for gibbsite, and 0.35 μmol m^{-2} for montmorillonite (Table II). The spectra of crystalline $Ni(OH)_2$ and takovite are shown for comparison. One can observe a strong XAFS signal out to higher energies, which indicates the presence of heavy back-scatterer elements such as Ni. There is an obvious similarity among the spectra of Ni sorption samples and the spectrum of takovite, a mixed Ni/Al hydroxide compound (Figure 8).

Figure 9 illustrates radial structure functions (RSFs) produced by forward Fourier transforms of the XAFS spectra represented in Figure 8 (*16*). The spectra were uncorrected for phase shift. All spectra showed a peak of R ≈ 1.8Å, which represents the first coordination shell of Ni. A second peak representing the second Ni shell can be observed at R ≈ 2.8Å in the spectra of the Ni sorption samples and takovite (Figure 9). These spectra also showed peaks beyond the second shell at R ≈ 5-6Å (Figure 9); these peaks resulted from multiple scattering among Ni atoms (*12*).

The structural parameters derived from XAFS analysis are summarized in Table II (*16*). Least-square fits of filtered XAFS for the first RSF peak reveal that in the first coordination shell Ni is surrounded by six O atoms. This behavior indicates that Ni(II) is in an octahedral environment. The Ni-O distances for the Ni sorption samples are 2.02-2.03Å and are similar to those in takovite (2.03Å). The Ni-O distances in crystalline $Ni(OH)_2$(s) are distinctly longer (2.06Å).

For the second shell, best fits were obtained by including both Ni and Si or Al as second-neighbor backscatterer atoms. Because Si and Al differ in atomic number by 1 (Z = 14 and 13, respectively), backscattering is similar. They cannot be easily distinguished from each other as second-neighbor backscatterers, especially in circumstances such as this where the contribution of both is small and cannot be resolved from each other in the Fourier transform.

The data analysis reveals 2.8 (montmorillonite) to 5.0 (gibbsite) Ni second-neighbor (N) atoms, indicative of the presence of Ni-nucleation products (see Table II). No correlation between the Ni surface sorption densities, Γs, and

Table I. Radii of Metal Cations[a]

Metal	Å
Al^{3+}	0.54[b]
Cd^{2+}	0.95
Co^{2+}	0.75
Cu^{2+}	0.73
Pb^{2+}	1.19
Ni^{2+}	0.69
Ti^{4+}	0.61
Zn^{2+}	0.74

[a] From Shannon (*77*)

[b] Radii for octahedral coordination

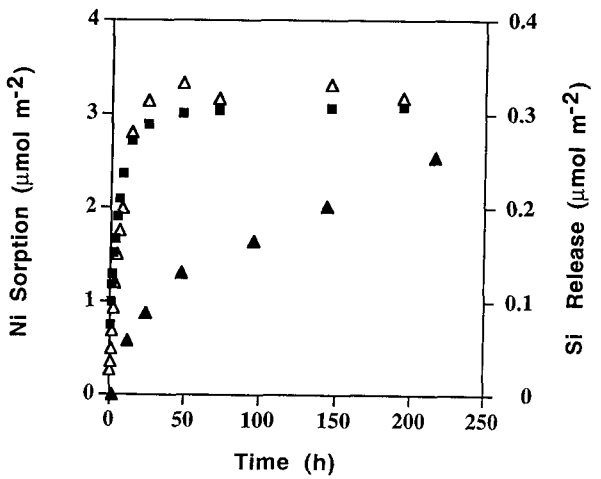

Figure 7. The kinetics of Ni sorption on pyrophyllite from a 3m*M* Ni solution at pH 7.5. (■) denotes the amount of sorbed Ni (μmol m^{-2}) and (△) the amount of simultaneous dissolved Si (μmol m^{-2}). The dissolution of untreated pyrophyllite at pH 7.5 is shown for comparison (▲). From Scheidegger et al. (*16*), with permission.

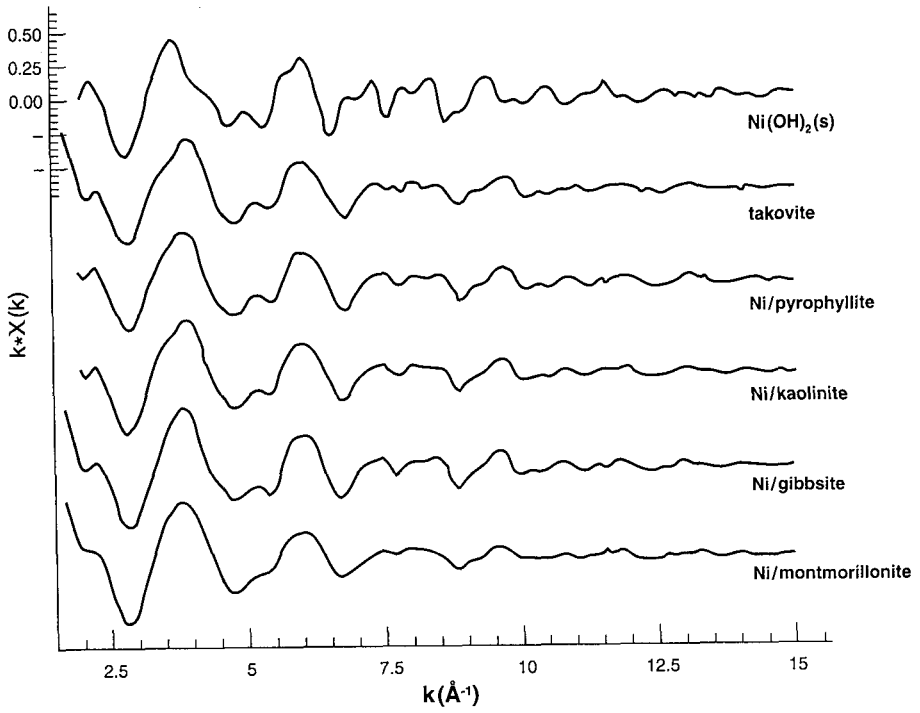

Figure 8. k-Weighted, normalized, background-subtracted XAFS spectra of Ni sorbed on pyrophyllite, kaolinite, gibbsite, and montmorillonite compared to the spectrum of crystalline $Ni(OH)_2$(s) and takovite. Reaction conditions are those given in 7. The spectra are uncorrected for phase shift. From Scheidegger et al. (*16*), with permission.

Table II. Structural Information Derived From XAFS Analysis Using EXCURVE[a,b].

		Ni-O			Ni-Ni			Ni-Si/Al			
	Γ μmol/m²	R(Å)	N	2σ²	R(Å)	N	2σ²	R(Å)	N	2σ²	N(Ni)/N (Si/Al)
$Ni(OH)_2$		2.06	6.0	0.011	3.09	6.0	0.010				
Takovite		2.03	6.0	0.01	3.01	3.1	0.009	3.03	1.1	0.009	2.8
Pyrophyllite	3.1	2.02	6.1	0.01	3.00	4.8	0.009	3.02	2.7	0.009	1.8
Kaolinite	19.9	2.03	6.1	0.01	3.01	3.8	0.009	3.02	1.8	0.009	2.2
Gibbsite	5.0	2.03	6.5	0.01	3.02	5.0	0.009	3.05	1.8	0.09	2.7
Montmorillonite	0.35	2.03	6.3	0.01	3.03	2.8	0.011	3.07	2.0	0.015	1.4

[a] From Scheidegger et al. (*16*)

[b] Interatomic distances (R, Å), coordination numbers (N), and Debye-Waller factors ($2\sigma^2$, Å²). The reported values are accurate to within R±0.02 Å, $N_{(Ni-O)}$ ±20%, $N_{(Ni-Ni)}$±40%, $N_{(Ni-Si/Al)}$±40%.

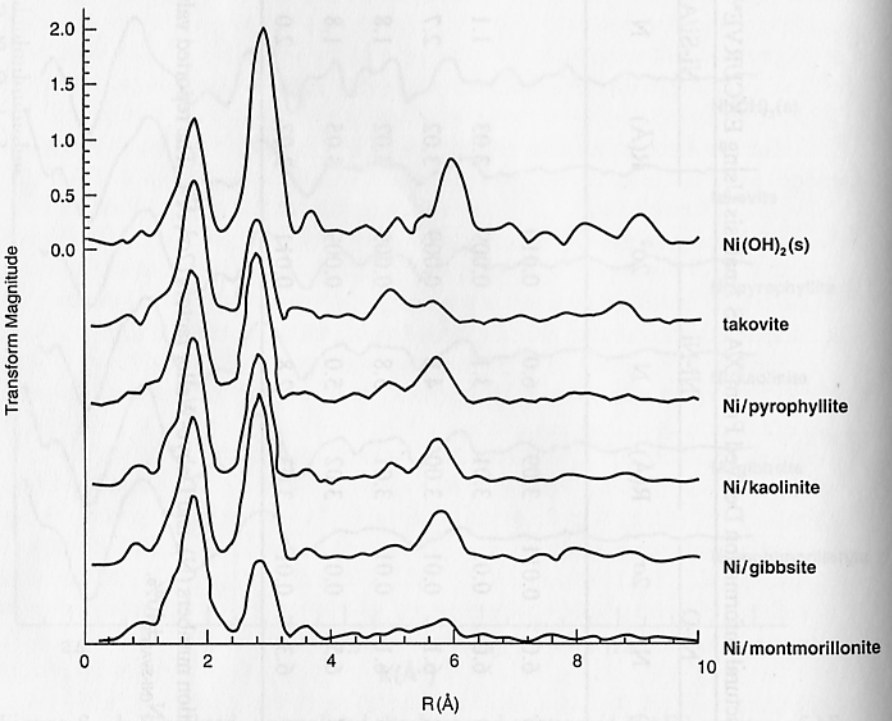

Figure 9. Radial structure functions (RSFs) produced by forward Fourier transforms of Ni sorbed on pyrophyllite, kaolinite, gibbsite, and montmorillonite compared to the spectrum of crystalline $Ni(OH)_2$(s) and takovite. The spectra are uncorrected for phase shift. From Scheidegger et al. (*16*), with permission.

the Ns of the Ni sorption samples is evident. Observed Ni-Ni distances (3.00-3.03Å) are similar to those in takovite (3.01Å), but distinctly shorter (0.06-0.08Å) than those in crystalline $Ni(OH)_2$(s) (3.09Å). XAFS data also reveal the presence of 1.8-2.7 Si/Al second-neighbor atoms at 3.02-3.07Å. Again, the bond distances are in good agreement with the Ni-Al distances observed in takovite (3.03Å).

Nickel sorption on pyrophyllite, kaolinite, gibbsite, and montmorillonite at pH 7.5 results in formation of Ni-nucleation products from solutions which are undersaturated with respect to the thermodynamic solubility product of $Ni(OH)_2$(s). An important finding of the study of Scheidegger et al. (*16*) is that the structural environment of Ni in all Ni sorption samples is similar. There is also an obvious similarity among the spectra of the Ni sorption samples and the spectrum of takovite, suggesting the presence of Ni phases of similar structure (Table II).

The existence of mixed-cation hydroxide phases has been reported in the literature (*72,73*). These compounds consist of structures in which divalent and trivalent metal ions are randomly distributed within the same brucite-like octahedral hydroxide layer. The general chemical formula for the compounds is $[Me^{2+}_{1-x}\,Me^{3+}_{x}(OH)_2]^{+x}\bullet(x/n)A^{-n}\bullet mH_2O$, where, for example, Me^{2+} is Mg(II), Ni(II), Co(II), Zn(II), Mn(II), and Fe(II), and Me^{3+} is Al(III), Fe(III), and Cr(III). The compounds exhibit a net positive charge x per formula unit which is balanced by an equal negative charge from interlayer anions A^{-n} such as Cl^-, Br^-, I^-, NO^-_3, OH^-, ClO^-_4, and CO_3^{2-}; water molecules occupy the remaining interlayer space (*73*). The octahedral layers can be stacked with hexagonal symmetry and two layers per unit cell, with rhombohedral symmetry and three layers per unit cell, or with less symmetrical arrangements (*74*). Minerals with the chemical formula given above are classified as the pyroaurite-sjoegrenite group (*75*). Natural pyroaurite and sjoegrenite are polymorphs having the composition $Mg_6Fe_2(OH)_{16}CO_3\bullet 4H_2O$. The minerals takovite, $Ni_6Al_2(OH)_{16}CO_3\bullet H_2O$, and hydrotalcite, $Mg_6Al_2(OH)_{16}CO_3\bullet H_2O$, are among the most common natural mixed-cation hydroxide compounds containing Al (*16,73*).

The synthesis of mixed-cation hydroxide compounds can be performed by induced hydrolysis (*73*). When a suspension of a fully hydrolyzed cation is added to a solution of another cation, and the pH is maintained constant and slightly below the value at which the second cation hydroxide would precipitate, hydrolysis of the solution cation followed by the precipitation of a fully hydrolyzed mixed-cation hydroxide compound would occur (*16*). In the experiment of Scheidegger et al. (*16*), Al was the fully hydrolyzed cation (see discussion below), Ni was the second cation, and the pH was maintained constant with the pH-stat apparatus at about 0.5 pH units below the pH where the precipitation of $Ni(OH)_2$ would be expected in homogeneous solution.

In the literature mixed Ni/Al compounds have been synthesized containing Cl^-, Br^-, OH^-, ClO_4^-, and CO^{2-}_3 (*72,73*). In the systems of Scheidegger et al. (*16*) the anions present were NO^-_3 and OH^- (NaOH was used to maintain a constant pH). Dissolved Al could not be detected in the samples, a necessity for the formation of mixed Ni/Al compounds. Even so, Al could have been released into solution and incorporated into mixed (Al and Si) hydroxides (*16*). Indeed, the

macroscopic data presented in Figure 7 suggest that surface complexes of Ni on pyrophyllite and kaolinite destabilize surface metal ions (Al and Si) relative to the bulk solution, and therefore lead to an enhanced dissolution of the clay. The association of Ni with Al could explain why the enhanced dissolution rate is only observable where Ni sorption is pronounced (see Figure 7).

The importance of Al in immobilizing heavy metals was recently pointed out by Lothenbach et al. (*76*). They studied the sorption kinetics of Cd, Cu, Pb, Ni, and Zn on montmorillonite, Al-montmorillonite and Al_{13}-montmorillonite. Addition of Al enhanced metal sorption of Ni and Zn and sorption increased with time, while Pb and Cd sorption were not affected by addition of Al. This finding agrees with the results of a recent XAFS study with Pb in our laboratory. No nucleation products seem to occur with Pb at surface loadings on clay minerals and γ-Al-oxide where nuclation products have been observed with smaller metals such as Co, Cu and Ni (Strawn, D. G., The University of Delaware, unpublished data). This sorption behaviour of Pb appears to be related to the mismatch in size between Pb^{2+} (1.19Å), and Al^{3+} (0.54Å) that is contained in the structure of the clay minerals and Al-oxide. The Pb ion is too large to fit into the mineral structure, while ions such as Ni^{2+} (0.69Å) and Co^{2+} (0.75Å) can fit into the structure (Table I).

To determine the formation kinetics of mixed Ni-Al hydroxide phases, Scheidegger et al. (*17*) used XAFS to spectroscopically monitor the sorption of Ni and formation of the phases with time on pyrophyllite. Figure 10 shows RSFs produced by forward Fourier transforms of the normalized, background-subtracted and k^3-weighted XAFS spectra of Ni sorbed on pyrophyllite for reaction times of 15 minutes, 75 minutes, 3 hours, 12 hours, 24 hours, and 3 months. The spectra are uncorrected for phase shift. All spectra show a peak of R ≈ 1.8Å, representing the first coordination shell of Ni. A second peak representing the second Ni coordination shell can be observed at R ≈ 2.8Å in the spectra of all Ni sorption samples. As reaction time progressed, and relative Ni removal from solution increased, the peak at R ≈ 2.8Å in the RSFs increased in intensity. This finding suggests the formation of Ni-nucleation products increasing in size with increasing reaction time.

The structural parameters derived from XAFS analysis for Ni/pyrophyllite are shown in Table III (*17*). In the first coordination shell Ni is surrounded by 6 O atoms, indicating that Ni(II) is in an octahedral environment. The Ni-O bond distance (≈ 2.05Å) and coordination numbers were not affected by the reaction time.

Data analysis of the second coordination shell revealed that the number of second-neighbor Ni atoms (N_{Ni-Ni}) increased with increasing time for pyrophyllite (Table III). N_{Ni-Ni} increased from N = 1.4-4.5 as the reaction time increased from 15 minutes to 3 months while the number of second-neighbor Al atoms increased from 1.5 to 2.4. Data in Table III also further reveal that the Ni-Ni bond distances (2.99Å-3.03Å) were essentially unaffected by the reaction time.

The growth of mixed Ni/Al phases on mineral surfaces was investigated spatially using SFM (Figure 11). A one cm^3 cube of pyrophyllite was reacted with Ni for various times using a pH-stat batch reactor (pH ≈ 7.5). At each time, the

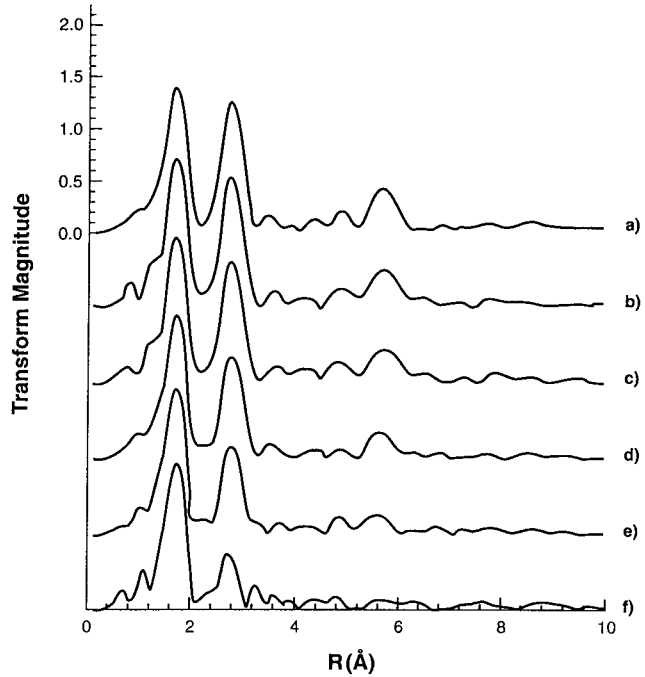

Figure 10. Radial structure functions (RSFs) of pyrophyllite samples reacted with Ni (reaction conditions are those given in Fig. 7) for a) 3 mo, b) 24 h, c) 12 h, d) 3 h, e) 75 min, and f) 15 min. The spectra are uncorrected for phase shift. Note the appearance of a peak at a R of about 2.8Å with increasing reaction time. From Scheidegger et al. (*17*), with permission.

Table III. Structural Information Derived From XAFS Analysis Using EXCURVE[a,b].

			Ni-O			Ni-Ni			Ni-Si/Al		
	relative Ni removal (%)	sorption density, Γ μmol/m²	R(Å)	N	2σ²	R(Å)	N	2σ²	R(Å)	N	2σ²
15 min	28	0.7	2.03	6.0	0.009	2.99	1.4	0.007	2.96	1.5	0.004
75 min	44	1.1	2.03	6.4	0.01	3.01	3.1	0.009	3.04	1.6	0.01
3 h	67	1.7	2.02	6.2	0.009	3.03	3.4	0.01	3.07	1.6	0.011
12 h	93	2.4	2.03	6.4	0.01	3.02	4.1	0.009	3.07	2.1	0.009
24 h	97	2.6	2.03	6.5	0.01	3.02	4.2	0.01	3.07	1.8	0.013
3 mo		3.1	2.03	6.5	0.01	3.02	4.5	0.011	3.07	2.4	0.016

[a] From Scheidegger et al. (*17*)

[b] Interatomic distances (R, Å), coordination numbers (N), and Debye-Waller factors (σ^2, Å^2). The reported values are accurate to within R±0.02 Å, $N_{(Ni\text{-}O)}$±20%, $N_{(Ni\text{-}Ni)}$±20%, $N_{(Ni\text{-}Si/Al)}$±40%.

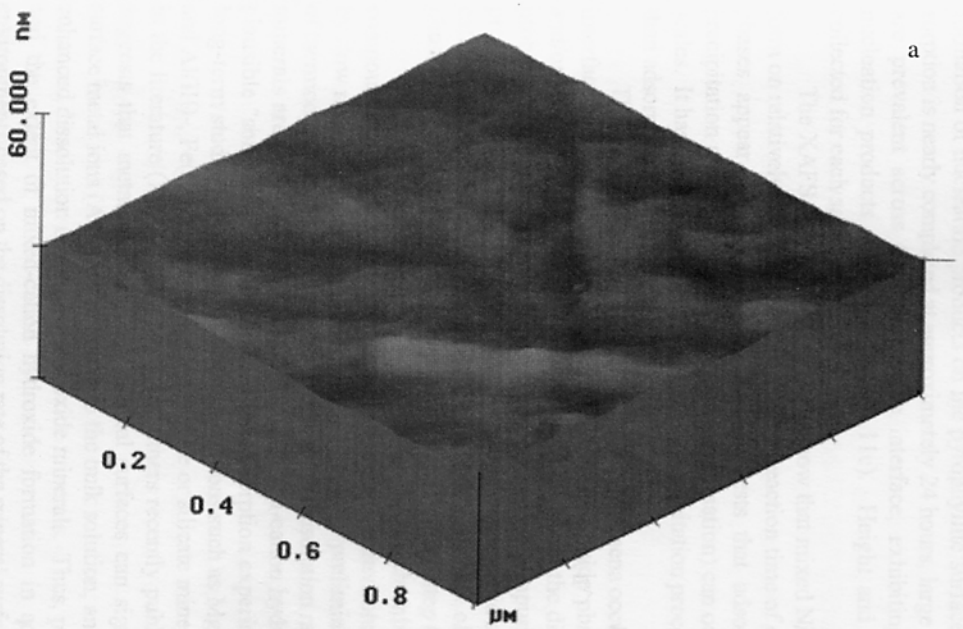

Figure 11. Scanning forces micrographs (SFM) of pyrophyllite (a) unreacted, (b) reacted for 1 h with Ni (pH 7.5, $[Ni]_o$ = 3 m*M*) , and (c) reacted for 24 h). The scan size was 1 μm X 1 μm with a maximum Z-range of 60 nm. The micrographs were collected with Tapping Mode© SFM (Scheckel, K. G., The University of Delaware, unpublished data).

Continued on next page.

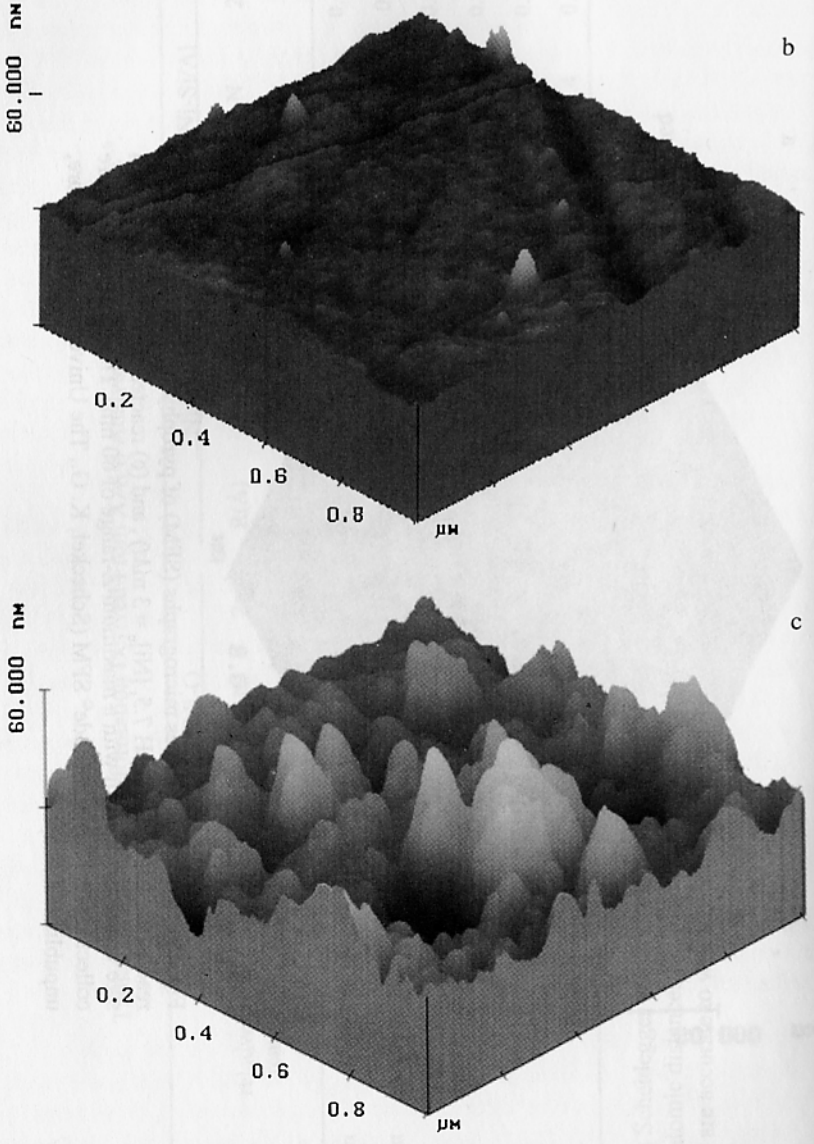

Figure 11. *Continued.*

sample was removed from the reactor and examined by SFM. The samples were scanned with a Digital Instruments Nanoscope IIIa SFM under TappingMode© AFM using multiple fresh tips. Each scan was run under the same parameters: the scan size for each image was 1 μm and the height range was 60 nm. Data in Figure 11 are presented in height mode only. Figure 11a shows the polished pyrophyllite surface prior to reaction with Ni. As the reaction progresses to one h, one begins to see the formation of nucleation products on the pyrophyllite surface (Figure 11b). When sorption is nearly completed at approximately 24 hours, large mountainous features are prevalent across the pyrophyllite interface, exhibiting the growth of the nucleation products with time (Figure 11c). Height and amplitude data were collected for each sample.

The XAFS and AFM data clearly show that mixed Ni-Al hydroxide phases form on relatively rapid time scales. After a reaction time of only 15 minutes, such phases appear on pyrophyllite. This suggests that adsorption and "surface" precipitation processes (mixed Ni/Al phase formation) can occur over similar time scales. It has traditionally been thought that precipitation processes are much slower than adsorption phenomena.

These above studies suggest that three phenomena occur at the mineral/liquid interface to cause formation of mixed-cation hydroxide phases: (1) non-specific and/or specific adsorption; (2) dissolution of Al where the dissolution rate is most probably dependent on the surface morphology and impurities present; and (3) precipitation of a mixed Ni/Al phase. The last step is rapid and proceeds until the cation concentrations correspond to the solubility product of the hydrotalcite-like phase. Dissolution of Al appears to be the rate-limiting step (*16,17*).

It has been proposed that the extent to which mixed-cation hydroxide compounds actually do form in aquatic and terrestrial environments is limited more by slow rates of soil mineral dissolution, a necessary preliminary step, than by lack of thermodynamic favorability (*51*). Because the dissolution rates of clays and oxide minerals are fairly slow, the possibility of mixed-cation hydroxide formation as a plausible "sorption mode" in 24 hour-based sorption experiments (and also most long-term studies) containing divalent metal ions such as Mg, Ni, Co, Zn, and Mn and Al(III)-, Fe(III)-, and Cr(III)-(hydr)oxide or silicate minerals has been ignored in the literature (*16,17*). This study and others recently published (*71*), however, suggests that metal sorption onto mineral surfaces can significantly destabilize surface metal ions (Al and Si) relative to the bulk solution, and therefore lead to an enhanced dissolution of the clay and oxide minerals. Thus, predictions on the rate and the extent of mixed-cation hydroxide formation in aquatic and terrestrial environments based on the dissolution rate of the mineral surface alone are not valid and underestimate the true values.

The studies of Scheidegger et al. (*16,17*) have emphasized the importance of combining time-dependent or kinetic studies with spectroscopic and microscopic investigations to better understand sorption processes at the soil mineral/water interface. Such studies can result in a detailed mechanistic understanding (e.g., distinguishing the rate of metal adsorption versus precipitation processes in sorption systems) which would be difficult to determine using a macroscopic approach alone.

Acknowledgments

We gratefully acknowledge the financial assistance of the DuPont Co., The State of Delaware, and the USDA (NRICGP), for their support of research reported in this review. Immense gratitude is extended to Dr. Noel C. Scrivner of the DuPont Co. for his unfailing support and encouragement during the past 10 years and to Dr. Robert G. Ford for his careful and thoughtful critique.

Literature Cited

1. Stumm, W.; Morgan, J. J. *Chemistry of the Solid-Water Interface*, 2nd ed.; Wiley: New York, NY, 1981.
2. Scheidegger, A.M.; Sparks, D.L. *Soil Sci.* **1996**, *161*, 813-831.
3. Goldberg, S. In *Advances in Agronomy*; Sparks, D. L., Ed.; Academic Press: San Diego, CA, 1992, Vol. 47; pp. 233-329.
4. Westall, J. C.; Hohl, H. *Adv. Colloid Interf. Sci.* **1980**, *12*, 265-294.
5. Farley, K. J.; Dzombak, D. A.; Morel, F. M. M. *J. Colloid Interf. Sci.* **1985**, *106*, 226-242.
6. James, R. O.; Healy, T. W. *J. Colloid Interf. Sci.* **1972**, *41*, 65-80.
7. Dzombak, D. A.; Morel, F. M. M. *Surface Complexation Modeling, Hydrous Ferric Oxide*, Wiley: New York, NY, 1990.
8. Katz, L. E.; Hayes, K. F. *J. Colloid Interf. Sci.* **1995**, *170*, 477-490.
9. Katz, L. E.; Hayes, K. F. *J. Colloid Interf. Sci.* **1995**, *170*, 491-501.
10. Fendorf, S. E.; Lamble, G. E.; Stapleton, M. G.; Kelley, M. J.; Sparks, D. L. *Environ. Sci. Technol.* **1994**, *28*, 284-289.
11. O'Day, P. A.; Brown, G. E., Jr.; Parks, G. A. *J. Colloid Interf. Sci.* **1994**, *165*, 269-289.
12. O'Day, P. A.; Parks, G. A.; Brown, G. E., Jr. *Clays Clay Miner.* **1994**, *42*, 337-355.
13. Papelis, C.; Hayes, K. F. *Coll. Surfaces.* **1996**, *107*, 89-96.
14. Scheidegger, A. M.; Lamble, G. M.; Sparks, D. L. *Environ. Sci. Technol.* **1996**, *30*, 548-554.
15. Scheidegger, A. M.; Fendorf, M.; Sparks, D. L. *Soil Sci. Soc. Am. J.* **1996**, *60*, 1763-1772.
16. Scheidegger, A. M.; Lamble, G. M.; Sparks, D. L. *J. Colloid Interf. Sci.* **1997**, *186*, 118-128.
17. Scheidegger, A. M.; Lamble, G. M.; Sparks, D. L. *J. Phys. IV France* **1997**, *7*, C2-773-775.
18. Johnston, C. T.; Sposito, G.; Earl, W. L. In *Environmental Particles*; Buffle, J.; vanLeeuwen, H. P., Eds.; Lewis Publ: Boca Raton, FL, 1993, pp. 1-36.
19. Koppelmann, M. H.; Emerson, A. B.; Dillard, J. G. *Clays Clay Miner.* **1980**, *28*, 119-124.
20. Dillard, J. G.; Koppelmann, M. H. *J. Colloid Interf. Sci.* **1982**, *95*, 298-309.
21. Schenk, C. V.; Dillard, J. G. *J. Colloid Interf. Sci.* **1983**, *95*, 398-409.
22. Hochella, M. F., Jr.; Carim, A. H. *Surf. Sci.* **1988**, *197*, 260-268.

23. Davison, N.; Whinnie, W. R. *Clays Clay Miner.* **1991**, *39*, 22-27.
24. Stipp, S. L., Hochella, M. F., Jr. *Geochim. Cosmochim. Acta.* **1994**, *58*, 3023-3033.
25. Scheidegger, A. M.; Borkovec, M.; Sticher, H. *Geoderma* **1993**, *58*, 43-65.
26. Junta, J. L.; Hochella, M. F., Jr. *Geochim. Cosmochim. Acta.* **1994**, *58*, 4985-4999.
27. Wersin, P.; Hochella, M. F., Jr.; Persson, P.; Redden, G.; Leckie, J. O.; Harris, D. W. *Geochim. Cosmochim. Acta.* **1994**, *58*, 2829-2843.
28. Papelis, C. *Environ. Sci. Technol.* **1995**, *29*, 1526-1533.
29. Perry, D. L.; Taylor, A.; Wagner, C. D. In *Instrumental Surface Analysis of Geologic Materials*; Perry, D. L., Ed.; VCH Publishers: New York, NY, 1990, pp. 45-86.
30. Fendorf, S. E.; Sparks, D. L.; Lamble, G. M.; Kelley, M. J. *Soil Sci. Soc. Am. J.* **1994**, *58*, 1583-1595.
31. Hochella, M. F., Jr. In *Spectroscopic Methods in Mineralogy and Geology*; Hawthorne, F. C., Ed.; Reviews in Mineralogy 18; Mineralogical Society of America: Washington, DC, 1988, pp. 573-630.
32. Hochella, M. F., Jr. In *Mineral-Water Interface Geochemistry*; Hochella, M. F., Jr.; White, A. F., Eds.; Reviews in Mineralogy 23; Mineralogical Society of America: Washington, DC, 1990, pp. 87-132.
33. Brown, G. E., Jr. In *Mineral-Water Interface Geochemistry*; Hochella, M. F., Jr.; White, A. F., Eds.; Reviews in Mineralogy 23; Mineralogical Society of America: Washington, DC, 1990, pp. 309-353.
34. Brown, G. E., Jr.; Parks, G. A.; Chisholm-Brause, C. J. *Chimia* **1989**, *43*, 248-256.
35. Charlet, L.; Manceau, A. In *Environmental Particles*; Buffle, J.; vanLeeuwen, H. P., Eds., Lewis Publ: Boca Raton, FL, 1993, pp. 117-164.
36. Schulze, D. G.; Bertsch, P. M. In *Advances in Agronomy*; Sparks, D. L., Ed.; Academic Press: San Diego, CA, 1995, *Vol.* 55; pp. 1-66.
37. Scheidegger, A. M.; Sparks, D. L. *Soil Sci. Soc. Am. J.* **1996**, *60*, 1763-1772.
38. Dove, P. M.; Chermak, J. A. In *Scanning Probe Microscopy of Clay Minerals*; Blum, A. E.; Nagy, K., Eds.; Clay Minerals Soc.: Boulder, CO, 1994, pp. 149-169.
39. Hochella, M. F., Jr. In *Mineral Surfaces*; Vaughn, D. J.; Pattrick, R. A. D., Eds.; Chapman and Hall: New York, NY, 1995, pp. 17-60.
40. Maurice, P. A. In *Environmental Particles*; Huang, P. M.; Senesi, N.; Buffle, J., Eds.; Wiley: New York, NY, 1998, Vol. 4; *In Press.*
41. Maurice, P. A. In *Advances in Agronomy*; Sparks, D. L., Ed.; Academic Press: San Diego, CA, 1997, *Vol.* 62; pp. 1-43.
42. Sparks, D. L. *Kinetics of Soil Chemical Processes*; Academic Press: San Diego, CA, 1989.
43. Jardine, P. M.; Sparks, D. L. *Soil Sci. Soc. Am. J.* **1984**, *48*, 39-45.
44. Comans, R. N. J.; Hockley, D. E. *Geochim. Cosmochim. Acta.* **1992**, *56*, 1157-1164.

45. Hachiya, K.; Sasaki, M.; Ikeda, J.; Mikami, N.; Yasunaga, T. *J. Phys. Chem.* **1984**, *88*, 27-31.
46. Hayes, K. F.; Leckie, J. O. In *Geochemical Processes at Mineral Surfaces*; Davis, J. A.; Hayes, K. F., Eds.; Am. Chem. Soc. Symp. Ser. 323; Am. Chem. Soc.: Washington, DC, 1986, pp. 114-141.
47. Grossl, P. R.; Sparks, D. L.; Ainsworth, C. C. *Environ. Sci. Technol.* **1994**, *28*, 1422-1429.
48. Bunzl, K.; Schmidt, W.; Sansoni, B. *J. Soil Sci.* **1976**, *27*, 32-41.
49. Sparks, D. L. In *Environmental Particles*; Huang, P. M.; Senesi, N.; Buffle, J., Eds.; Wiley: New York, NY, *Vol.* 4; *In Press*.
50. Strawn, D. G.; Sparks, D. L. In *Fate and Transport of Metals in the Vadose Zone*; Selim, H. M.; Iskandar, A., Eds.; Lewis Publishers: Boca Raton, FL, 1998, *In Press*.
51. McBride, M. B. *Environmental Chemistry of Soils*; Oxford Univ. Press: New York, NY, 1994.
52. Ainsworth, C. C.; Pilou, J. L.; Gassman, P. L.; Van Der Sluys, W. G. *Soil Sci. Soc. Am. J.* **1994**, *58*, 1615-1623.
53. Pignatello, J. J.; Xing, B. *Environ. Sci. Technol.* **1996**, *30*, 1-11.
54. Burgos, W. D.; Novak, J. T.; Berry, D. F. *Environ. Sci. Technol.* **1996**, *30*, 1205-1211.
55. Bruemmer, G. W.; Gerth, J.; Tiller, K. G. *J. Soil Sci.* **1988**, *39*, 37-52.
56. Coughlin, B. R.; Stone, A. T. *Environ. Sci. Technol.* **1995**, *29*, 2445-2455.
57. Axe, L.; Anderson, P. R. *J. Colloid Interf. Sci.* **1997**, *185*, 436-448.
58. Sposito, G. *The Chemistry of Soils*; Oxford Univ. Press: New York, NY, 1989.
59. McBride, M. B. *Clays Clay Miner.* **1982**, *30*, 21-28.
60. Lehmann, R. G.; Harter, R. D. *Soil Sci. Soc. Am. J.* **1984**, *48*, 769-772.
61. O'Day, P. A.; Chisholm-Brause, C. J.; Towle, S. N.; Parks, G. A.; Brown, G. E., Jr. *Geochim. Cosmochim. Acta.* **1996**, *60*, 2515-2532.
62. Chisholm-Brause, C. J.; O'Day, P. A.; Brown, G. E., Jr.; Parks, G. A.; Leckie, J. O. *Nature* **1990**, *348*, 528-530.
63. Chisholm-Brause, C. J.; Hayes, K. F.; Roe, A. L.; Brown, G. E., Jr.; Parks, G. A.; Leckie, J. O. *Geochim. Cosmochim. Acta.* **1990**, *54*, 1897-1909.
64. Roe, A. L.; Hayes, K. F.; Chisholm-Brause, C. J.; Brown, G. E., Jr.; Parks, G. A.; Hodgson, K. O.; Leckie, J. O. *Langmuir* **1991**, *7*, 367-373.
65. Charlet, L.; Manceau, A. *J. Colloid Interf. Sci.* **1992**, *148*, 443-458.
66. Bargar, J. R.; Brown, G. E., Jr.; Parks, G. A. 209th Am. Chem. Soc. National Meeting, extended abstracts, Vol. 35(1).
67. Towle, S. N.; Bargar, J. R.; Brown, G. E., Jr.; Parks, G. A. *J. Colloid Interf. Sci.* **1997**, *187*, 62-82.
68. Xia, K.; Mehadi, A.; Taylor, R. W.; Bleam, W. F. *J. Colloid Interf. Sci.* **1997**, *185*, 252-257.
69. Sposito, G. In *Geochemical Processes at Mineral Surfaces*; Davis, J. A.; Hayes, K. F., Eds.; Am. Chem. Soc. Symp. Ser. 323; Am. Chem. Soc.: Washington, DC, 1986, pp. 217-228.

70. Magini, M.; Licheri, G.; Paschina, G.; Piccaluga, G.; Pirna, G. *X-ray Diffraction of Ions in Aqueous Solutions: Hydration and Complex Formation*; CRC Press: Boca Raton, FL. 1988.
71. d'Espinose de la Caillerie, J. B.; Kermarec, M.; Clause, O. *J. Am. Chem. Soc.* **1995**, *117*, 11471-11481.
72. Allmann, R. *Chimia* **1970**, *24*, 99-108.
73. Taylor, R. M. *Clay Miner.* **1984**, *19*, 591-603.
74. Brindley, G. W.; Kikkawa, S. *Am. Mineral.* **1979**, *64*, 836-843.
75. Hashi, K.; Kikkawa, S.; Koizumi, M. *Clays Clay Miner.* **1983**, *31*, 152-154.
76. Lothenbach, B.; Furrer, G.; Schulin, R. *Environ. Sci. Technol.* **1997**, *31*, 1452-1462.
77. Shannon, R. D. *Acta Cryst.* **1976**, *A32*, 751-767.
78. Hayes, K. F. Ph.D. Dissertation, Stanford University. **1987**.